Applied Mathematical Modelling 97 (2021) 483–500

Contents lists available at ScienceDirect

Applied Mathematical Modelling

journal homepage: www.elsevier.com/locate/apm

Dynamic stability of an electromagnetic suspension maglev vehicle under steady aerodynamic load

Han Wu[a,b], Xiao-Hui Zeng[a,b,*], Ding-Gang Gao[c], Jiang Lai[d]

[a] Key Laboratory for Mechanics in Fluid Solid Coupling Systems, Institute of Mechanics, Chinese Academy of Sciences, Beijing, China
[b] School of Engineering Science, University of Chinese Academy of Sciences, Beijing, China
[c] Maglev Transportation Engineering R&D Center, Tongji University, Shanghai, China
[d] Nuclear Power Institute of China, Chengdu, China

ARTICLE INFO

Article history:
Received 21 August 2020
Revised 2 April 2021
Accepted 10 April 2021
Available online 24 April 2021

Keywords:
EMS maglev vehicle
Dynamic stability
Aerodynamic load
Critical speed

ABSTRACT

In this study, the suspension stability of a maglev vehicle is investigated under steady aerodynamic load. The dynamics of the maglev vehicle in the vertical direction are modelled by considering aerodynamic lift and pitching moment, and this model is adopted to investigate how the aerodynamic load influences the suspension stability by analysing the critical speed by means of eigenvalue analysis and direct integration. Doing so reveals three modes of suspension failure: (i) an upward aerodynamic load or pitching moment can give rise to a dynamic instability, (ii) a downward aerodynamic load can give rise to a static instability and (iii) the electromagnet becomes locked in the guide-way because the vertical aerodynamic force borne by the electromagnet exceeds the vehicle weight borne by it, and the electromagnetic force cannot adjust the suspension gap. In essence, failure modes (i) and (ii) correspond to motion stability when the maglev vehicle system is perturbed by a small amount, whereas failure mode (iii) is similar to the electromagnet holding the track in the event of control failure, albeit by a different mechanism. Each suspension failure mode has its own critical speed, and how that speed depends on the aerodynamic coefficients and feedback control gains is determined.

1. Introduction

Electromagnetic suspension (EMS) maglev trains have many advantages over traditional wheel–rail trains, such as lower energy consumption, better climbing ability and less environmental impact [1], and they have undergone tremendous development in recent years. The design speed of China's new-generation high-speed maglev trains is 600 km/h, which exceeds the aircraft cruising speed. Predictably the aerodynamic load will have a non-negligible effect on their dynamic behaviours during high-speed maglev operation. The suspension of an EMS maglev train is realised by the attraction between an electromagnet and the guide-way. Because the attraction electromagnetic force is inversely proportional to the square of the suspension gap, an electromagnetic suspension is inherently unstable, and feedback control is essential to ensure the dynamic stability of the maglev vehicle system. Maintaining the dynamic stability of the maglev vehicle system is the primary condition for the safe and comfortable operation. How the vehicle, guide-way and control parameters affect the stability of

* Corresponding author at: Key Laboratory for Mechanics in Fluid Solid Coupling Systems, Institute of Mechanics, Chinese Academy of Sciences, Beijing, China.
E-mail address: zxh@imech.ac.cn (X.-H. Zeng).

https://doi.org/10.1016/j.apm.2021.04.008
0307-904X/

the maglev vehicle system, and how to improve that system's dynamic performance have been extensively investigated [2]. However, the aerodynamic effect on the dynamic stability of maglev system becoming more and more prominent as the speed of maglev train increases has been less observed, thereby it is the urgent need to do relevant research.

In recent years, more and more researchers have begun focusing on the aerodynamic loads on high-speed maglev trains and have analyzed the aerodynamic loads and pressure waves on maglev trains operating in open air and passing another train [3–8]. Moreover, a few studies on the dynamic responses of EMS maglev vehicle subjected to aerodynamic loads were reported. Kwon et al. [9] simulated the response of a maglev train to wind gusts, and the results showed that the low-frequency vibration caused by wind turbulence would degrade the ride comfort. Yau [10] calculated how a coupled vehicle–rail system would respond to an unsteady wind load, and they proposed a proportional-integral-derivative+linear quadratic regulator controller to reduce the acceleration response of the vehicle. Wu and Shi [11] simulated the dynamic response of a maglev vehicle under the action of a wind field, and they studied the influences of wind speed, vehicle speed and feedback control gains. Liu and Tian [12] simulated the transverse vibration response when two maglev vehicles pass each other in open air, and Takizawa [13] studied the comfort for passengers when two MLX01 maglev trains pass each other at 500 km/h.

These works took aerodynamic load as external excitation to study the forced vibration response of maglev train under aerodynamic load. In essence, the effect of aerodynamic load was only reflected in the addition of a non-homogeneous term which represents the forced excitation to the right side of the dynamic equation. Non-homogeneous term does not change the inherent characteristics of the system represented by the terms on the left side of the dynamic equation. However, the dynamic stability of a maglev vehicle considering aerodynamic load is a problem of self-excited vibration, the stability characteristics of self-excited vibration cannot be obtained using the analysis results of forced vibration. Aerodynamic load can also change the stiffness and damping matrices on the left side of the dynamic equation, so that the inherent characteristics of the dynamic system of maglev train will be changed. Therefore, the aerodynamic load can change the self-excited vibration characteristics of the high-speed maglev train, and then lead to the change of the motion stability, critical speed and the corresponding instability mode. The change of the self-excited vibration characteristics caused by aerodynamic load has not been recognized in the previous studies.

Stable levitation of an EMS high-speed maglev vehicle depends on a controlled vertical electromagnetic force. Because maglev train are basically symmetrical, the aerodynamic force on the lateral direction is very small when running on the open line [14], and its influence on the vertical suspension stability can be ignored. In addition, the vertical aerodynamic load is very large, which can reach 50% of the vehicle weight [6]. Therefore, compared with the lateral aerodynamic force, the vertical aerodynamic force (e.g. aerodynamic lift and aerodynamic pitching moment) affects the dynamic stability more significantly. The present authors established a single-electromagnet suspension model considering aerodynamic lift and proposed a new concept of the critical speed of the maglev system [15]. However, in Ref. [15], a single-degree-of-freedom model was used, and only vertical aerodynamic lift was considered in the model, but no aerodynamic pitching moment. It is obvious that the single-degree-of-freedom model in Ref. [15] is only applicable to the introduction of basic concepts and the establishment of research ideas, not applicable to the quantitative study of vehicle instability characteristics under the aerodynamic lift and moment.

In view of discuss above, a vertical dynamic model of maglev vehicle under aerodynamic lift and pitching moment is established in this paper. The influence of the aerodynamic lift and pitching moment on the equilibrium state current of each electromagnet is taken into account, then the model is linearized at the equilibrium position. Based on the linear model, the instability mechanism of maglev vehicle under aerodynamic lift and pitching moment is investigated by means of numerical integration and eigenvalue analysis, and three instability modes are clarified. In addition, the relationships between critical speed and aerodynamic coefficients and feedback control gains are obtained.

2. System model

2.1. Vehicle dynamic model

A high-speed EMS maglev vehicle can be equivalent to the vertical suspension model [16] shown in Fig. 1. As shown in Fig. 1, the vehicle structure is simplified as a rigid car body connected by second suspensions to four rigid maglev frames, each of which contains four electromagnets. Because the stiffness of primary suspension is very large, and it is two orders of magnitude larger than the second suspension, the relative displacement of the electromagnet and the maglev frame is very small. Therefore, the primary suspension is neglected, and the guide-way is assumed to be rigid. In this paper, the vertical suspension stability of maglev vehicle is studied, so only the heaving and pitching motion of the vehicle body and the maglev frame are considered. Aerodynamic lift and pitching moment act on the car body. The nominal suspension clearance of the electromagnet is set as δ_0. When the vehicle is undisturbed and the aerodynamic force is steady, the balance of electromagnetic force, gravity and aerodynamic force is achieved at the stable suspension gap. At this case, the current in the electromagnet is set as I_0, and the position of car body and maglev frames is $\mathbf{x}_0$. The motion of the vehicle system with respect to $\mathbf{x}_0$ can be expressed as

$$\mathbf{x}_v = \begin{bmatrix} z_c & \theta_c & z_{c1} & \theta_{c1} & z_{b2} & \theta_{b2} & z_{b3} & \theta_{b3} & z_{b4} & \theta_{b4} \end{bmatrix}^T, \tag{1}$$

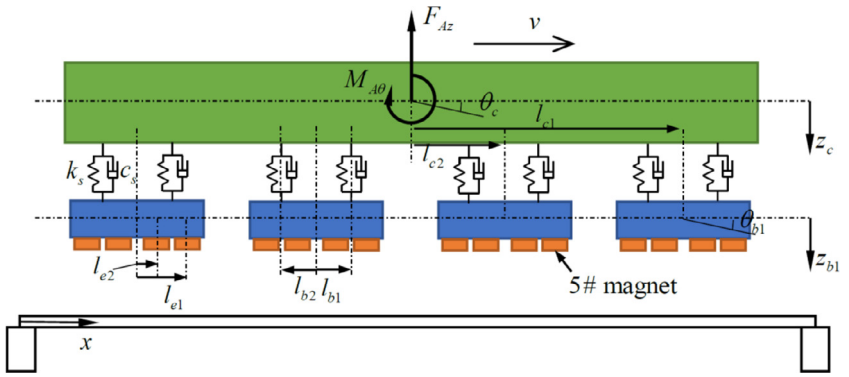

Fig. 1. Maglev vehicle dynamic model with 10 degrees of freedom (DOF).

where z_c and θ_c are the heave and pitch, respectively, of the car body and z_{bj} and θ_{bj} are the heave and pitch, respectively, of the maglev frame j (j = 1– 4).

The vehicle dynamics model is established near the equilibrium position $\mathbf{x}_0$, which is expressed as

$$\begin{aligned} m_c\ddot{z}_c &= -\sum_{j=1}^{4}\sum_{i=1}^{2}\begin{bmatrix} k_s\left[z_c+\left(l_{cj}+l_{bi}\right)\theta_c-z_{bj}-l_{bi}\theta_{bj}\right] \\ +c_s\left[\dot{z}_c+\left(l_{cj}+l_{bi}\right)\dot{\theta}_c-\dot{z}_{bj}-l_{bi}\dot{\theta}_{bj}\right]\end{bmatrix} \\ I_c\ddot{\theta}_c &= -\sum_{j=1}^{4}\sum_{i=1}^{2}\left(l_{cj}+l_{bi}\right)\begin{bmatrix} k_s\left[z_c+\left(l_{cj}+l_{bi}\right)\theta_c-z_{bj}-l_{bi}\theta_{bj}\right] \\ +c_s\left[\dot{z}_c+\left(l_{cj}+l_{bi}\right)\dot{\theta}_c-\dot{z}_{bj}-l_{bi}\dot{\theta}_{bj}\right]\end{bmatrix} \end{aligned} \tag{2}$$

for the car body and

$$\begin{aligned} m_b\ddot{z}_{bj} &= \sum_{i=1}^{2}\begin{bmatrix} k_s\left(z_c+\left(l_{cj}+l_{bi}\right)\theta_c-z_{bj}-l_{bi}\theta_{bj}\right) \\ +c_s\left(\dot{z}_c+\left(l_{cj}+l_{bi}\right)\dot{\theta}_c-\dot{z}_{bj}-l_{bi}\dot{\theta}_{bj}\right)\end{bmatrix}-\sum_{k=1}^{4}\Delta F_{mjk} \quad j=1\sim 4 \\ I_b\ddot{\theta}_{bj} &= \sum_{i=1}^{2}l_{bi}\begin{bmatrix} k_s\left(z_c+\left(l_{cj}+l_{bi}\right)\theta_c-z_{bj}-l_{bi}\theta_{bj}\right) \\ +c_s\left(\dot{z}_c+\left(l_{cj}+l_{bi}\right)\dot{\theta}_c-\dot{z}_{bj}-l_{bi}\dot{\theta}_{bj}\right)\end{bmatrix}-\sum_{k=1}^{4}l_{ek}\Delta F_{mjk} \quad j=1\sim 4 \end{aligned} \tag{3}$$

for the maglev frames. In Eqs. (2) and (3), note that the heave and pitch of the car body and each maglev frame are the fluctuations away from the steady-state equilibrium positions under aerodynamic load, gravity and electromagnetic force. ΔF_{mjk} is the fluctuation of the electromagnetic force of electromagnet k on maglev frame j. Meanings of other variables parameters are shown in Appendix 1.

2.2. Aerodynamic force model

The speed of reverse airflow of high speed maglev train is much larger than the speed of crosswind, and it plays a dominant role in the aerodynamic load of maglev train. In addition, this paper focuses on the effect of the aerodynamic lift and pitch moment on vertical suspension stability, the aerodynamic lift and pitch moment mainly produced by reverse airflow of high speed maglev train. Therefore, the crosswind is neglected, and only the oncoming steady airflow at the front of the maglev train is considered herein. The aerodynamic lift F_{Az} and the aerodynamic pitching moment $M_{A\theta}$ are taken as steady loads at a given speed v, which are expressed as

$$\begin{aligned} F_{Az} &= \frac{1}{2}C_L\rho A_v v^2, \\ M_{A\theta} &= \frac{1}{2}C_\theta\rho A_v L v^2, \end{aligned} \tag{4}$$

where ρ is the air density (1.225 kg/m^3), A_v is the cross sectional area, L is the reference height of the vehicle's mass centre, C_L is the coefficient of aerodynamic lift and C_θ is the coefficient of aerodynamic pitching moment.

2.3. Electromagnetic force model

The electromagnetic force of electromagnet k on frame j is calculated using

$$F_{m,jk} = \frac{\mu_0 A_m {N_m}^2\left(I_{0,jk}+i_{jk}\right)^2}{4\left(\delta_{0,jk}+s_{jk}\right)^2}, \tag{5}$$

where A_m is the effective area of the electromagnet, N_m is the number of coil turns, μ_0 is the magnetic permeability of air, $I_{0,jk}$ is the stable current, $\delta_{0,jk}$ is the stable suspension clearance and i_{jk} and s_{jk} are the fluctuations of the current and the suspension clearance, respectively.

The electromagnetic force is linearized at electromagnetic equilibrium position ($I_{0,jk}$, $\delta_{0,jk}$),

$$\begin{aligned} F_{mjk} &= \frac{\mu_0 AN^2}{4{\delta_{0,jk}}^2}\left({I_{0,jk}}^2 + 2I_{0,jk}i + {i_{jk}}^2\right)\left[1 + 2\left(-\frac{s_{jk}}{\delta_{0,jk}}\right)^1 + 3\left(-\frac{s_{jk}}{\delta_{0,jk}}\right)^2 \cdots\right] \\ &\approx \frac{\mu_0 AN^2}{4{\delta_{0,jk}}^2}\left({I_{0,jk}}^2 + 2I_{0,jk}\cdot i_{jk}\right)\left(1 - \frac{2s_{jk}}{\delta_{0,jk}}\right) \\ &\approx F_{m0_{jk}} + \Delta F_{mjk} = F_{m0,jk} + k_{i,jk}\cdot i_{jk} - k_{c,jk}\cdot s_{jk}, \\ k_{i,jk} &= \frac{\mu_0 A_m {N_m}^2 I_{0,jk}}{2{\delta_{0,jk}}^2}, k_{c,jk} = \frac{\mu_0 A_m {N_m}^2 {I_{0,jk}}^2}{2{\delta_{0,jk}}^3}, I_{0,jk} = \frac{2\delta_{0,jk}}{N_m}\sqrt{\frac{F_{m0,jk}}{\mu_0 A_m}}, \end{aligned} \tag{6}$$

where $F_{m0,jk}$ is the electromagnetic force of magnet k on frame j at equilibrium. According to Eq. (6), the fluctuation of the electromagnetic force is expressed as

$$\Delta F_{mjk} = k_{i,jk} i_{jk} - k_{c,jk}\left(z_{bj} + l_{ek}\theta_{bj}\right). \tag{7}$$

The governing equation [17] of the magnetic-levitation control system is

$$\dot{i}_{jk} = \frac{k_i}{L_{0jk}}\cdot \dot{s}_{jk} - \frac{R}{L_{0jk}}\cdot i_{jk} + \frac{1}{L_{0jk}} u_{jk}, \tag{8}$$

where u_{jk} is the voltage fluctuation, L_0 is the electrical inductance and

$$L_{0jk} = \frac{\mu_0 AN^2}{2\delta_{0jk}}. \tag{9}$$

Eq. (8) can then be re-written as

$$\dot{i}_{jk} = \frac{k_{i,jk}}{L_{0,jk}}\cdot\left(\dot{z}_{bj} + l_{ek}\dot{\theta}_j\right) - \frac{R}{L_{0,jk}}\cdot i_{jk} + \frac{1}{L_{0,jk}} u_{jk}. \tag{10}$$

To facilitate the analysis of the instability mechanism of the maglev train when considering the aerodynamic lift, the following proportional-derivative controller is adopted to control the voltage of the electromagnet:

$$u_{jk} = k_p\left(z_{bj} + l_{ek}\theta_j\right) + k_d\left(\dot{z}_{bj} + l_{ek}\dot{\theta}_j\right). \tag{11}$$

In Eq. (11), k_p is the position feedback gain, and k_d is the velocity feedback gain.

2.5. The effect of aerodynamic lift and pitch moment on maglev dynamic system

Eq. (6) shows that the stable current $I_{0,jk}$ depends on the equilibrium-state suspension force, which is closely related to the steady aerodynamic lift and pitching moment. It means that the aerodynamic load influences the parameters of the suspension system. As shown in Eq. (4), the aerodynamic lift and moment are directly proportional to the square of the vehicle speed, and the influence of aerodynamic lift on the dynamic stability becomes more obvious as the vehicle speed increases.

When the aerodynamic load is neglected, one has $F_{m0,jk} = m_c g/16 + m_b g/4$ in the equilibrium state of the maglev vehicle. However, an aerodynamic load changes the equilibrium-state electromagnetic force. When the aerodynamic lift is considered, distributing the aerodynamic lift evenly among the electromagnets, the change in the equilibrium-state electromagnetic force is $-F_{AZ}/16$. When the aerodynamic pitching moment is considered, we assume the vehicle is deflected by a virtual pitch angle ε that causes a vertical displacement $(l_{cj} + l_{ek})\ \varepsilon$ for each electromagnet. For simplicity, it is assumed that the change of the equilibrium-state electromagnetic force due to the aerodynamic pitching moment is proportional to the virtual vertical displacement and that the resultant moment is M_{Az}:

$$\begin{aligned} \Delta F_{jk-MAz} &= \Delta F_{(j=2,k=4)-MAz}\times\frac{l_{cj}+l_{ek}}{l_{c2}+l_{e4}} = \frac{0.5\times M_{Az}}{\sum_{j=1}^{2}\sum_{k=1}^{4}\frac{\left(l_{cj}+l_{ek}\right)^2}{l_{c2}+l_{e4}}}\times\frac{l_{cj}+l_{ek}}{l_{c2}+l_{e4}}\quad (j=1,2) \\ \Delta F_{jk-MAz} &= \Delta F_{(j=3,k=1)-MAz}\times\frac{l_{cj}+l_{ek}}{l_{c3}+l_{e1}} = \frac{0.5\times M_{Az}}{\sum_{j=3}^{4}\sum_{k=1}^{4}\frac{\left(l_{cj}+l_{ek}\right)^2}{l_{c3}+l_{e1}}}\times\frac{l_{cj}+l_{ek}}{l_{c3}+l_{e1}}\quad (j=3,4) \end{aligned} \tag{12}$$

Considering the effects of the aerodynamic lift and pitching moment, the equilibrium-state electromagnetic force is expressed as

$$F_{m0,jk} = \frac{m_c g}{16} + \frac{m_b g}{4} - \frac{F_{Az}}{16} + \Delta F_{jk-MAz}. \tag{13}$$

Note that an electromagnet cannot provide a repulsive force in reaction to the guide-way. Therefore, to ensure that the electromagnets can be adjusted to provide suspension (or to ensure that sign of evolution in Eq. (6) is of practical engineering significance), the condition

$$F_{m0,jk} > 0 \tag{14}$$

must be met.

In general, the controller ensures that the stable suspension gap $\delta_{0,jk}$ of the electromagnet remains invariant; consequently, changing the equilibrium-state electromagnetic force changes the equilibrium-state current $I_{0,jk}$. The linear maglev vehicle system is obtained by linearizing the nonlinear system about the equilibrium position, and its characteristic parameters depend on the equilibrium state of the maglev vehicle system; that equilibrium state changes if the equilibrium-state current changes, as well as because of natural changes in the system parameters. When the maglev train exceeds a certain speed, the change of parameter due to the increased aerodynamic force gives rise to instability. Namely, the maglev train reaches a critical speed that exists only if aerodynamic forces are considered and is inconsistent with the critical speed of conventional wheel–rail trains.

2.6. State-space equation and stability analysis

The state-space equation of the vehicle under aerodynamic lift and pitch moment are obtained from the car-body vibration (Eq. (2)), the maglev-frame vibration

Eq. (3)), the electromagnetic force (Eqs. (6) and ((7)), the current (Eq. (10)) and the feedback control (Eq. (11)). Reducing their order, the linearized state-space equation can be expressed in

$$\begin{aligned} \dot{\mathbf{x}}(t) &= \mathbf{A}\cdot\mathbf{x}(t) + \mathbf{B}\cdot\mathbf{u}(t) \\ \mathbf{u}(t) &= \mathbf{K}\cdot\mathbf{x}(t) \end{aligned} \tag{15}$$

where, $\mathbf{x}(t)_{36\times1}$ is the vector of the system states, $\mathbf{u}(t)_{\ 36\times1}$is the vector of the voltages, $\mathbf{A}_{\ 36\times36}$, $\mathbf{B}_{36\times36}$ are the matrices of vehicle structure parameters and electromagnet, and $\mathbf{K}_{36\times36}$ is the vector of control gains.

The state vector is

$$\begin{aligned} \mathbf{x}(t) = \{&z_c, \dot{z}_c, \theta_c, \dot{\theta}_c, z_{b1}, \dot{z}_{b1}, \theta_{b1}, \dot{\theta}_{b1}, z_{b2}, \dot{z}_{b2}, \theta_{b2}, \dot{\theta}_{b2}, z_{b3}, \dot{z}_{b3}, \theta_{b3}, \dot{\theta}_{b3}, z_{b4}, \dot{z}_{b4}, \theta_{b4}, \dot{\theta}_{b4}, \\ &i_{11}, i_{12}, i_{13}, i_{14}, i_{21}, i_{22}, i_{23}, i_{24}, i_{31}, i_{32}, i_{33}, i_{34}, i_{41}, i_{42}, i_{43}, i_{44}\}^T \end{aligned} \tag{16}$$

the vector of the voltages is

$$\mathbf{u}(t) = \left\{ \overbrace{0, \cdots, 0}^{20}, u_{11}, u_{12}, u_{13}, u_{14}, u_{21}, u_{22}, u_{23}, u_{24}, u_{31}, u_{32}, u_{33}, u_{34}, u_{41}, u_{42}, u_{43}, u_{44} \right\}^T \tag{17}$$

The details of matrices **A, B** and **K** are shown in Appendix 2.

Based on eigenvalue analysis and numerical integration, we can obtain the speed where the maglev system become unstable, which is called the critical speed.

3. Simulation program and verification

The vehicle structural parameters and electromagnet parameters used in this study are determined according to appendix 2 of Ref. [18], as shown in Appendix 1. To ensure the correctness of the critical speed simulation program, the critical speed of a maglev vehicle considering aerodynamic lift is calculated using both eigenvalue analysis and numerical integration method. Fig. 2 shows how the real part of the maximum eigenvalue varies with the vehicle speed as calculated by eigenvalue analysis, and Fig. 3 shows the time history of suspension clearance calculated by direct integration, the critical speed obtained using these two approaches both are 518.9 km/h. The comparison verifies the correctness of these two programs.

In addition, to verify the correctness and reliability of the model in this paper, we simulated the vehicle body acceleration under random irregularity, and compared it with the results of Shi et al. [19], as shown in Fig. 4. Shi et al. simulated the dynamic response of the vehicle under random track irregularity and compared with the experimental results, but they did not consider the influence of aerodynamic loads in their study. The parameters used in comparison were consistent with Shi et al's study. The results of the model in this paper are close to the simulation results of Shi et al. and measured results, which indicates that the model in this paper can represent the vertical motion characteristics of vehicles.

4. Influence of aerodynamic coefficients on critical speed

This section analyses how the coefficients of aerodynamic lift and pitching moment influence the critical speed of the maglev vehicle. The following parameter values pertain to a TR08 maglev car on the Shanghai maglev line: $A_v = 11.86\ \mathrm{m}^2$, $L = 4.1$ m and $\rho = 1.225\ \mathrm{kg/m}^3$. For a three-car multiple train, the CFD simulation shows that the lift coefficients of the front, middle and rear cars are approximately 0.6, 0.1 and 0.35, respectively, if the train is running in open air at 600 km/h.

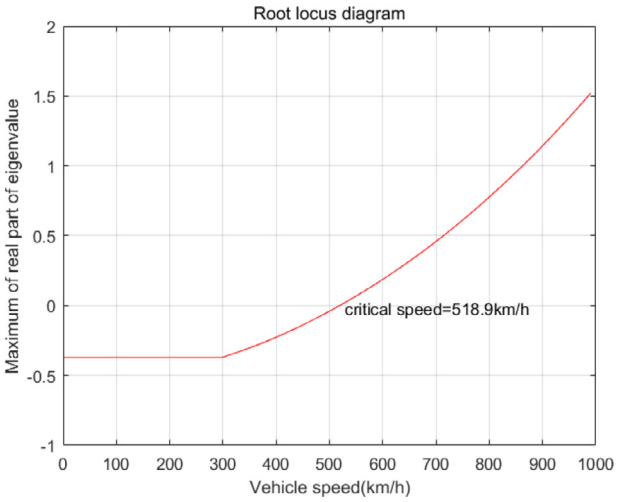

Fig. 2. Variation of the largest real part of the eigenvalue with vehicle speed (k_p = 1800, k_d = 200, C_L = 0.6 and C_θ = 0.0).

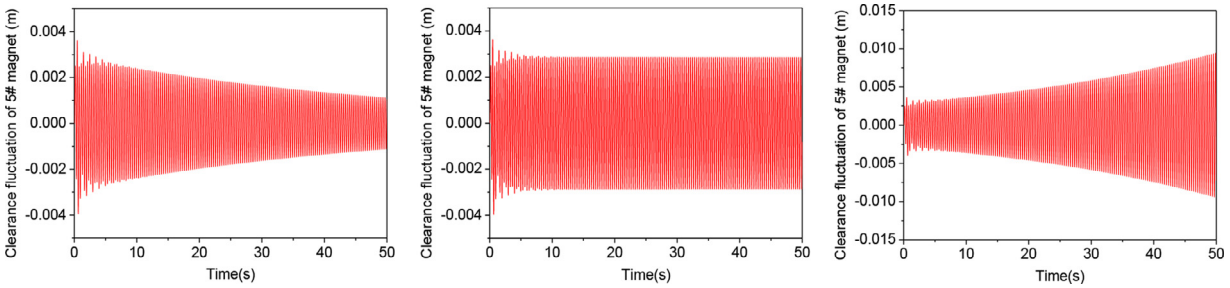

Fig. 3. Time history of clearance fluctuation at (a) 510 km/h; (b) 518.9 km/h; and (c) 530 km/h . (k_p = 1800, k_d = 200, C_L = 0.6 and C_θ = 0.0).

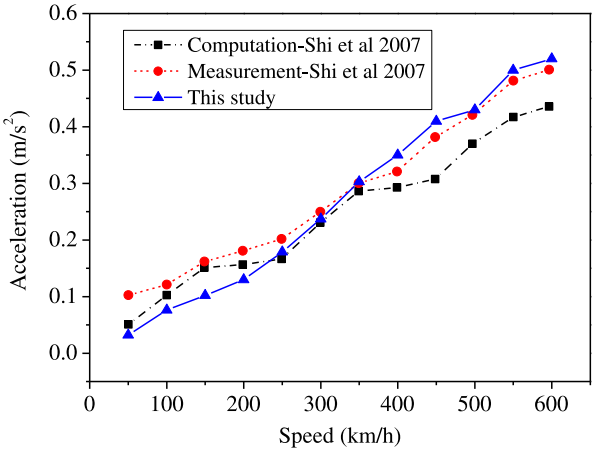

Fig. 4. Comparison of vehicle acceleration.

Furthermore, the coefficients of the pitching moment of the front, middle and rear cars are approximately 1.0, 0.035 and 0.78, respectively. Therefore, to analyse fully the laws that govern the influences of aerodynamic lift and pitching moment, the range of both coefficients is selected as 0.4–1.8. Aerodynamic lift is considered as either upward lift or downward lift, and pitching moment is considered as either bending moment or heading moment.

Table 1 shows that, the larger the aerodynamic lift coefficient, the lower the critical speed of the maglev vehicle. When the aerodynamic lift is upward, the critical speed is generally lower than that when the lift is downwards, indicating that the maglev vehicle is more prone to instability under upward aerodynamic lift.

The variation of critical speed with positive and negative pitching coefficient is shown in Table 2.

Table 1
critical speed under different lift coefficients.

lift coefficient	Critical speed under upward lift		Critical speed under downward lift	
	k_p=1800, k_d=200	k_p =1400, k_d =160	k_p =1800, k_d =200	k_p =1400, k_d =160
0.4	635.6	761.0	1696.1	927.1
0.6	518.9	621.4	1384.8	757.0
0.8	449.4	538.1	1199.3	655.6
1	402.0	481.3	1072.7	586.3
1.2	367.0	439.4	979.2	535.5
1.4	339.7	406.8	906.6	495.5
1.6	317.8	380.5	848.0	463.5
1.8	299.6	358.8	799.5	437.0

Table 2
Critical speed under different pitching coefficients.

lift coefficient	Critical speed under positive pitching moment		Critical speed under negative pitching coefficient	
	k_p =1800, k_d =200	k_p =1400, k_d =160	k_p =1800, k_d =200	k_p =1400, k_d =160
0.3	1388.9	1162.4	1388.9	1162.4
0.4	1202.8	1006.7	1202.8	1006.7
0.5	1075.8	900.4	1075.8	900.4
0.6	982.1	822.0	982.1	822.0
0.7	909.2	761.0	909.2	761.0
0.8	850.5	711.8	850.5	711.8
0.9	801.8	671.1	801.9	671.1
1	760.7	636.7	760.7	636.7
1.1	725.3	607.1	725.3	607.1
1.2	694.4	581.2	694.4	581.2
1.3	667.2	558.4	667.2	558.4
1.4	642.9	538.1	642.9	538.1
1.5	621.1	519.9	621.1	519.9
1.6	601.4	503.4	601.4	503.4
1.7	583.4	488.3	583.4	488.3
1.8	567	474.6	567	474.6

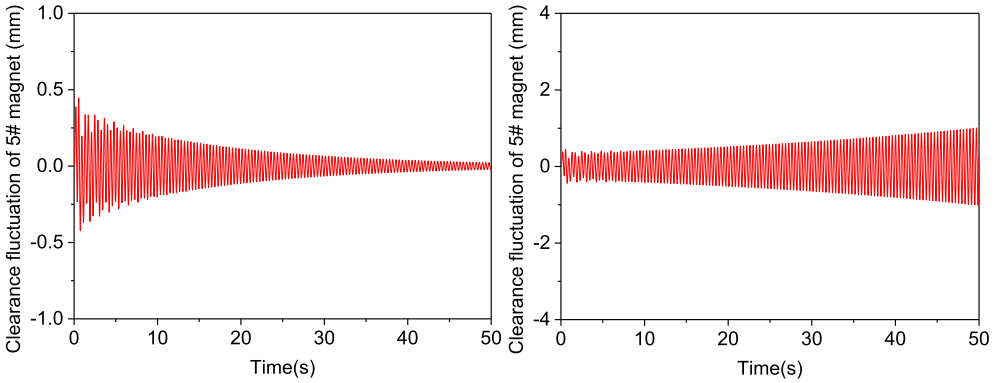

Fig. 5. Time history of clearance of magnet 5 at (a) 600 km/h and (b) 630 km/h (critical speed: 621.4 km/h; C_L = 0.6, k_p = 1400 and k_d = 160).

The results show that, the larger the aerodynamic pitching moment, the lower the critical speed. Furthermore, under the same conditions, the calculated critical speed is the same regardless of whether the aerodynamic pitching moment is positive or negative, thereby indicating that the direction of the aerodynamic pitching moment does not affect the critical speed.

5. Instability mechanism

According to the analysis in Section4, the critical speed does not depend on the direction of the aerodynamic pitching moment but does depend on the direction of the aerodynamic lift. In this section, the instability mechanism under different aerodynamic conditions is studied.

The dynamic response of the maglev vehicle near its critical speed is simulated using the dynamic response simulation program when the initial value z_{b1}=0.1 mm is given. According to the results shown in Fig. 5, when the maglev vehicle

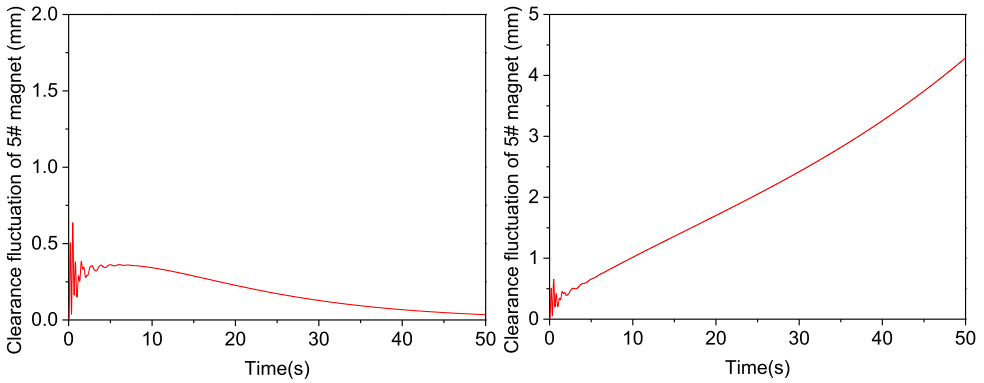

Fig. 6. Time history of clearance of magnet 5 at (a) 735 km/h and (b) 765 km/h (critical speed: 757.0 km/h; $C_L = -0.6$, $k_p = 1400$ and $k_d = 160$).

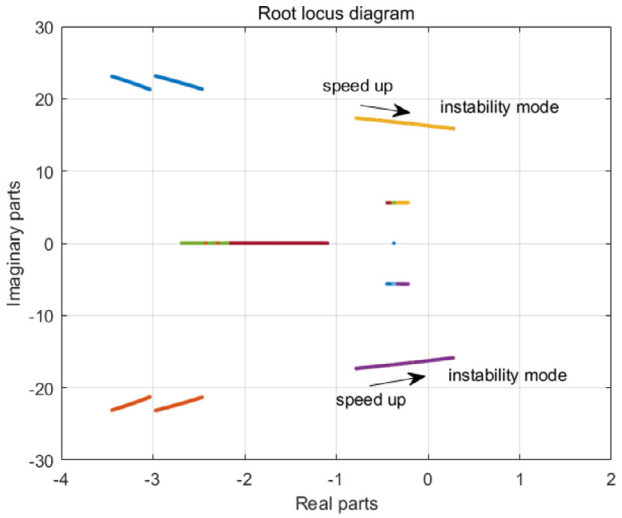

Fig. 7. Root locus diagram (critical speed: 621.4 km/h; $k_p = 1400$, $k_d = 160$, $C_L = 0.6$ and $C_\theta = 0.0$).

experiences a positive (upward) aerodynamic lift, it will oscillate under disturbance. If the vehicle speed is less than the critical speed, then the vibration amplitude of the vehicle attenuates gradually. However, if the vehicle speed exceeds the critical speed, then the vibration amplitude of the vehicle increases gradually and becomes unstable.

In the case of negative (downward) aerodynamic lift, the maglev vehicle will deviate from the equilibrium position and oscillate barely when the system is disturbed. This deviation converges gradually to zero, and the system is stable, if the vehicle speed is less than the critical speed, as shown in Fig. 6(a). However, if the speed exceeds the critical speed, then the deviation increases gradually without converging, and the system is unstable, as shown in Fig. 6(b).

The results in Figs. 5 and 6 indicate that the instability forms under positive lift and negative lift are totally different. Why the instability mode differs with a positive or negative aerodynamic lift is analysed using the root locus diagrams. As shown in Fig. 7 and Fig. 8, the eigenvalues of the system can be divided into two categories, one is the complex (the vertical coordinate is not zero) and the other is the real (the vertical coordinate is zero, that is, the imaginary part of eigenvalue is zero). In Fig. 7, with the increase of speed, the real part of the complex eigenvalue gradually increases and exceeds zero. Fig. 8 indicates that the real eigenvalue gradually increases and exceeds zero with the increase of speed.

According to the stability theory of linear system, when the eigenvalue is the conjugate complex, the imaginary part represents the oscillation process; if the real part is less than zero, the equilibrium position is a stable focus, and the amplitude of the system decays exponentially, as shown in Fig. 5(a). When the real part is greater than zero, the equilibrium position is an unstable focus, and the amplitude of the system increases exponentially, as shown in Fig. 5(b).

If the eigenvalue is real and there is no imaginary part, the system will not oscillate. If it is less than zero, the equilibrium position is a stable node, and the solution will approach the equilibrium position in an exponential form (Fig. 6(a)); if it is greater than zero, it is an unstable node; the solution will not oscillate and increase in an exponential form (Fig. 6(b)).

Therefore, when considering the positive (upward) aerodynamic lift and pitching moment, the dynamic instability will come out when the maglev system reaches the critical speed, while the static instability occurs if considering the negative (downward) lift force. The instability modes are different.

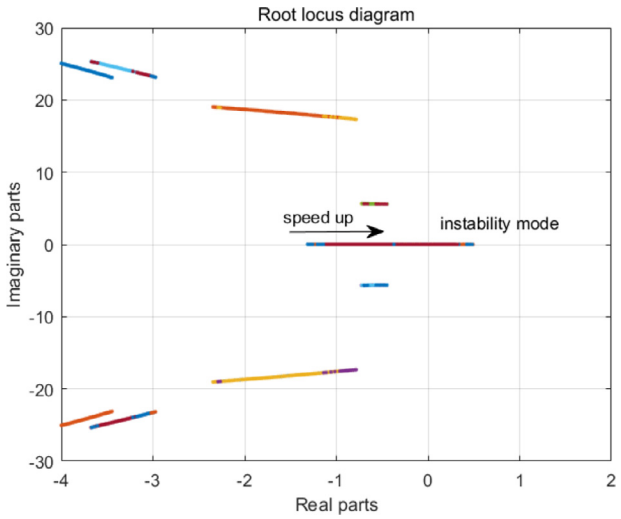

Fig. 8. Root locus diagram (critical speed: 757.0 km/h; $k_p = 1400$, $k_d = 160$, $C_L = -0.6$ and $C_\theta = 0.0$).

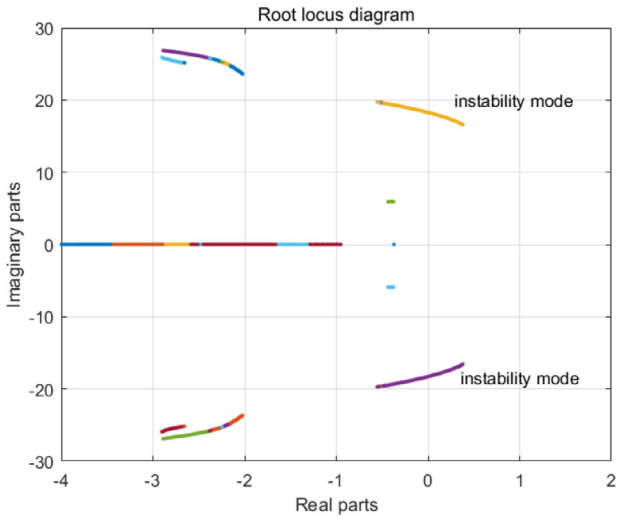

Fig. 9. Root locus diagram (critical speed: 760.7 km/h; $k_p = 1800$, $k_d = 200$, $C_L = 0.0$ and $C_\theta = 1.0$).

The above analysis shows that the instability mode of the maglev vehicle system differs according to the aerodynamic lift directions. In addition, the root locus diagram in Fig. 9 shows that a dynamic instability occurs at the critical speed when the aerodynamic pitching moment is considered.

As we know, the PD controller cannot eliminate the levitation static error, which is a major problem for significant load perturbations. Therefore, once the critical speed is reached when the downward aerodynamic lift acts on the maglev train, the deviation gradually increases without converging, just as shown in Fig. 6(b). This may be the reason why the 'static instability' occurs. PID control algorithm is commonly adopted in practical maglev train. As a result of the existence of integral control term, the results shown in Fig. 6(b) will discontinue to exist when the critical speed is achieved; however, it will present a divergence with oscillation, as shown in Fig. 10(b). However, the oscillation shown in Fig. 10(b) originates from the integral control term in PID algorithm, and it is a process of adjusting static error. This belongs to static instability, which is extremely different from dynamic instability shown in Fig. 5(b).

The dynamic and static instabilities of a maglev vehicle subjected to an aerodynamic load can be classified according to the stability of a dynamical system subjected to disturbance. The stable solution means that the system deviates from the equilibrium position under the disturbance, it will automatically return to the equilibrium position, otherwise it is unstable. In other words, in these two cases, once the maglev vehicle has reached its critical speed, the vehicle movement cannot return to the equilibrium state if the vehicle is subjected to disturbance; Ideally, however, the vehicle will remain in its equilibrium position without other disturbances.

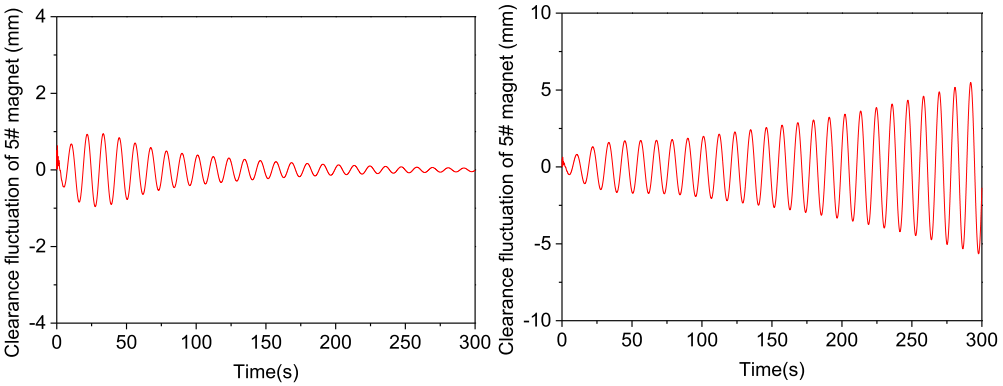

Fig. 10.. Time history of clearance of magnet 5 at (a) 750 km/h and (b) 760 km/h (critical speed: 757 km/h; C_L =− 0.6, k_p = 1400, k_i = 50 and k_d = 160, PID algorithm is adopted).

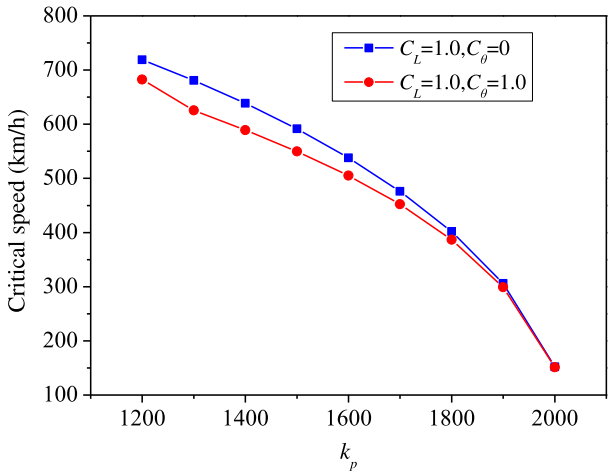

Fig. 11. Variation of critical speed with k_p (upward aerodynamic lift).

As well as the two suspension failure modes already discussed, it should be noted that a maglev vehicle subjected to an aerodynamic load can fail via a third mode. When an upward aerodynamic lift or pitching moment is considered, there is a certain speed at which the vertical aerodynamic force borne by the electromagnet exceeds the vehicle weight borne by it. At this speed, the equilibrium electromagnetic force is negative, thereby violating the requirement of Eq. (14). Because the EMS train can no longer provide a repulsive force between the electromagnet and the guide-way, the system cannot adjust the suspension gap, and the electromagnet will lock the guide-way.

Unlike the first two suspension failure modes, in the third failure mode, after the vehicle reaches the critical speed, the electromagnet will directly lock the guide-way even if there is no disturbance. This is similar to the phenomenon whereby the electromagnet locks the guide-way because of control failure, albeit the mechanism is completely different. The third failure mode also involves a critical speed. Obviously, the larger the aerodynamic coefficient, the lower the critical speed of the third failure mode.

6. Relationship between critical speed and control parameters

This section analyses how the critical speed depends on the position feedback control gain k_p and the velocity feedback control gain k_d.

6.1. Relationship between critical speed and position feedback control gain k_p

Figs. 11 and 12 show how the critical speed varies with the position feedback control gain when the aerodynamic lift is upward and downwards, respectively. On the basis of the instability-mechanism research in Section5, Fig. 11 shows that the dynamic-instability critical speed under upward aerodynamic lift is correlated positively with the position feedback control gain k_p. Meanwhile, Fig. 12 shows that the static-instability critical speed under downwards aerodynamic lift is correlated

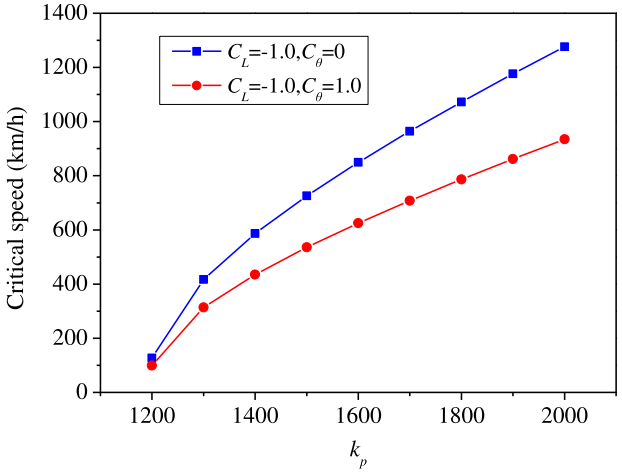

Fig. 12. Variation of critical speed with k_p (downward aerodynamic lift).

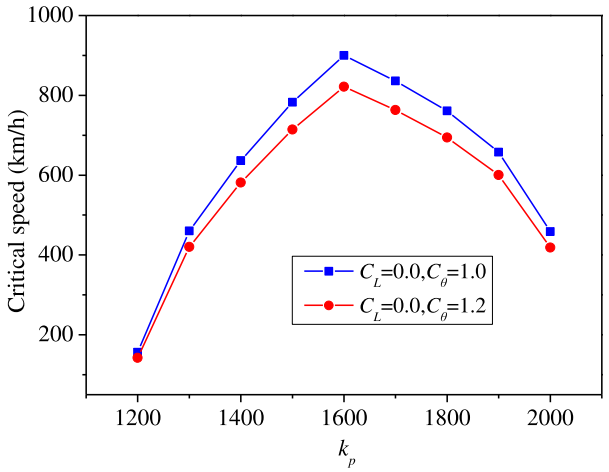

Fig. 13. Variation of critical speed with k_p (aerodynamic pitch force).

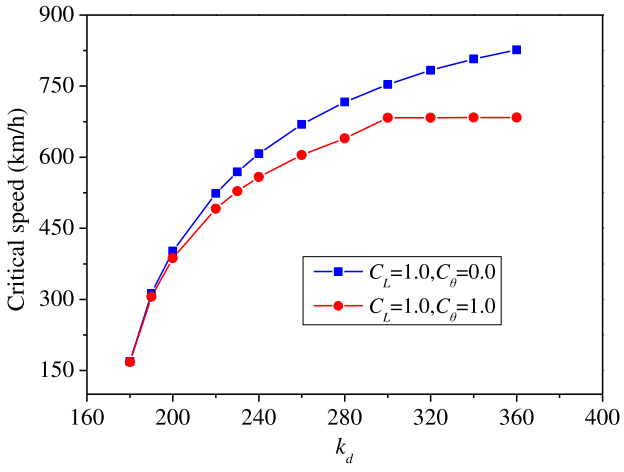

Fig. 14. Variation of critical speed with k_d (upward aerodynamic lift).

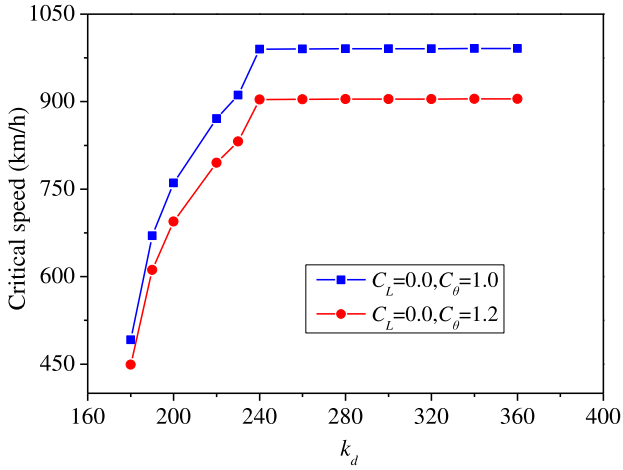

Fig. 15. Variation of critical speed with k_d (aerodynamic pitch force).

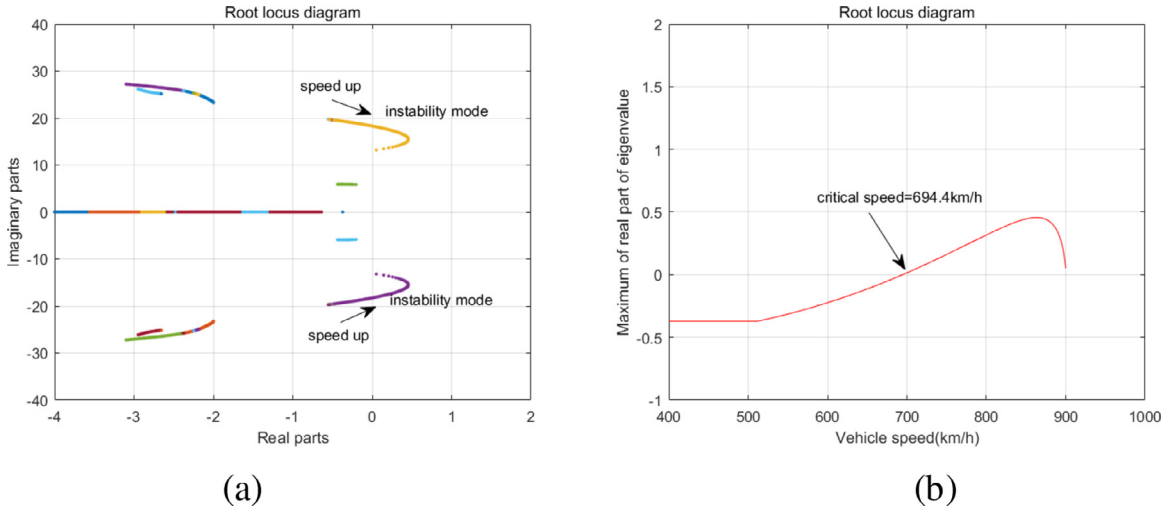

Fig. 16. (a): root locus diagram. (b): variation of the real part of the maximum eigenvalue with vehicle speed (k_p = 1800, k_d = 200, C_L = 0.0 and C_θ = 1.2).

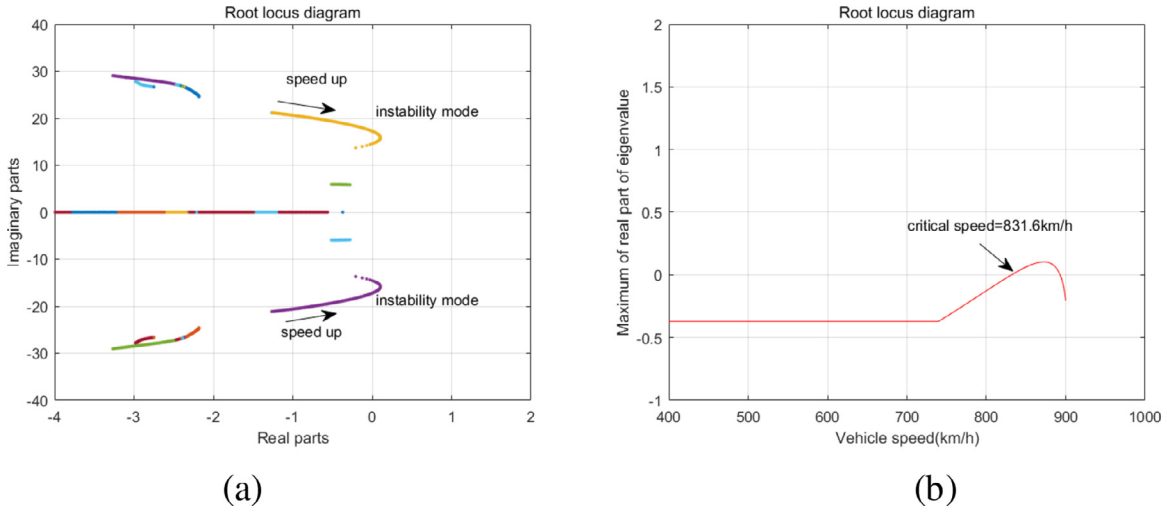

Fig. 17. (a): root locus diagram. (b): variation of the real part of the maximum eigenvalue with vehicle speed (k_p = 1800, k_d = 230, C_L = 0.0 and C_θ = 1.2).

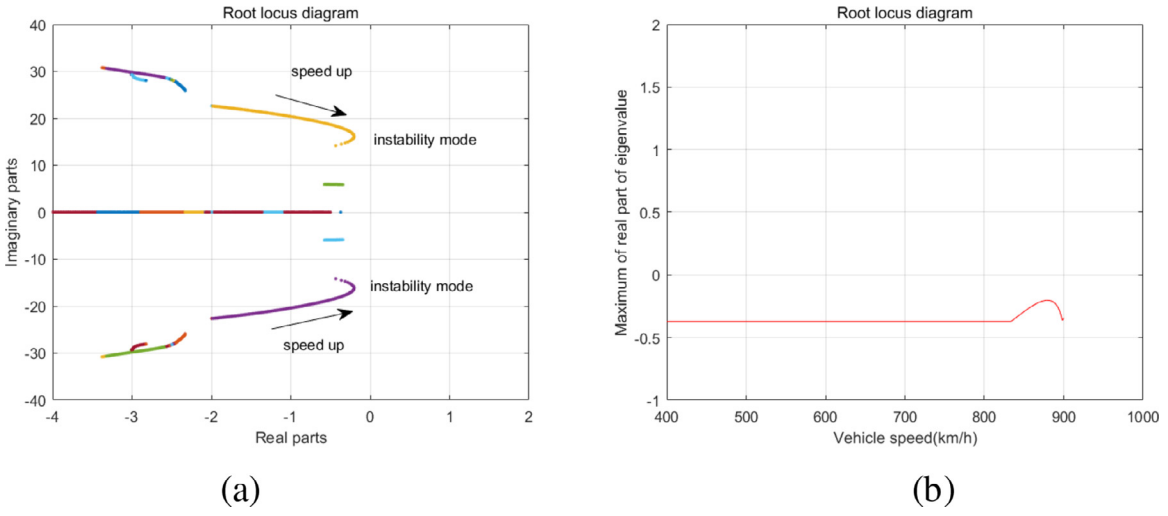

Fig. 18. (a): root locus diagram. (b): variation of the real part of the maximum eigenvalue with vehicle speed (k_p = 1800, k_d = 260, C_L = 0.0 and C_θ = 1.2).

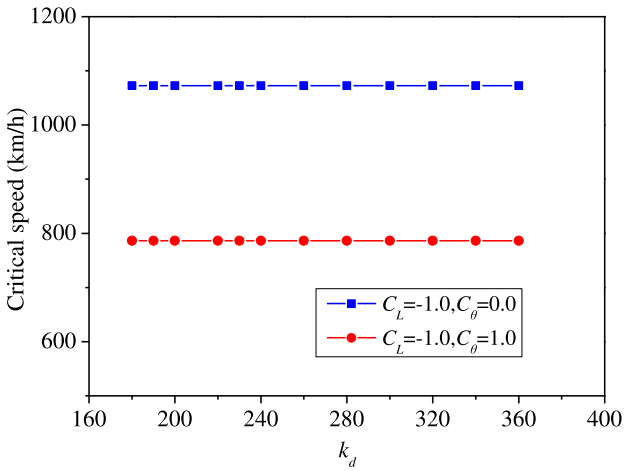

Fig. 19. Variation of critical speed with k_d (downward aerodynamic lift).

negatively with the position feedback control gain k_p. In addition, Fig. 13 shows that the dynamic-instability critical speed first increases and then decreases with k_p when the aerodynamic pitching moment is considered.

6.2. Relationship between critical speed and velocity feedback control gain k_d

Figs. 14 and 15 show how the critical speed varies with the velocity control gain k_d when upward aerodynamic lift and aerodynamic pitching moment are considered. Fig. 14 shows that the critical speed of the maglev vehicle increases monotonically with k_d when only upward aerodynamic lift is considered, whereas it first increases gradually with k_d and then basically remains unchanged when both upward aerodynamic lift and pitching moment are considered. Fig. 15 shows that, when only the aerodynamic pitching moment is taken into account, as k_d increases, the critical speed first increases gradually and then basically remains unchanged.

In view of this phenomenon wherein the critical speed first gradually increases and then basically remains unchanged, root loci are drawn for analysis when C_L = 0, C_θ = 1.2, k_d = 200, k_d = 230 and k_d = 260, as shown in Figs. 16–18. The results show that, when the aerodynamic pitching moment is considered, with the increase of speed, the real part of the eigenvalue of a certain mode of the maglev vehicle increases gradually to become non-negative and instability occurs if k_d is small, as shown in Figs. 16 and 17. Comparing the eigenvalue of this mode in Figs. 16–18 shows that, when k_d changes

gradually from 200 to 260, the real part of the eigenvalue keeps always negative with the vehicle speed increasing. Namely, at $k_d = 260$, this mode is no longer unstable.

For $k_p = 1800$, $k_d = 260$, $C_L = 0.0$ and $C_\theta = 1.2$, the critical speed is 904 km/h. The force of the electromagnet at this speed is analysed, and it is found that the upward aerodynamic force borne by the last electromagnet exceeds the weight and the equilibrium electromagnetic force is negative, indicating that this critical speed corresponds to the third failure mode.

In the equilibrium state, the vehicle weight borne by each electromagnet is known from Eq. (13). Therefore, the value of aerodynamic pitching moment which makes the electromagnet force negative can be obtained. When the aerodynamic pitching coefficient is determined, the vehicle critical speed in this situation is surely determined, which is independent of the control gains. Therefore, the critical speed of the maglev vehicle gradually become constant as k_d increases when the aerodynamic pitching is taken into account, as shown in Figs. 14 and 15.

According to the above analysis, if the aerodynamic lift is downwards, then static instability occurs at the critical speed. Fig. 19 shows that the static-instability critical speed does not depend on k_d.

7. Conclusions

This paper studies the suspension stability of a maglev vehicle under aerodynamic conditions based on a 10-DOF vertical dynamic model, and it reveals three suspension failure modes of a maglev vehicle when considering aerodynamic lift and pitching moment. The first one is dynamic instability, which occurs when upward aerodynamic lift or pitching moment is considered; in this mode, the vibration amplitude of the maglev vehicle increases indefinitely. The second one is static instability, which occurs when downward aerodynamic lift is considered; in this mode, the maglev vehicle does not vibrate, but its displacement keeps increasing. The third one is that the upward aerodynamic force borne by the electromagnet exceeds the vehicle's weight; the electromagnetic force cannot produce a repulsive force to adjust the suspension gap, and the electromagnet locks the guide-way. In essence, the first two failure modes can be classified as instability problems of a maglev vehicle system under disturbance. In these two cases, once the maglev vehicle has reached its critical speed, it can still run smoothly if it suffers no other disturbance. For the third failure mode, once the vehicle has reached its critical speed, the electromagnet will directly lock the guide-way even if there is no disturbance, and the maglev vehicle cannot run.

In addition, there is a critical speed corresponding to each of these three suspension failure modes, and the following rules on how these critical speeds vary are obtained.

(1) The larger the coefficients of aerodynamic lift and pitching moment, the lower the critical speed.
(2) The dynamic-instability critical speed decreases with the position feedback gain and increases with the velocity feedback gain when the aerodynamic lift is upward. The static-instability critical speed increases with the position feedback gain and is independent of the velocity feedback gain when the aerodynamic lift is downward. Considering the aerodynamic pitching moment, the critical speed first increases and then decreases with the position feedback gain. The instability mode differs according to the direction of the aerodynamic lift, whereas the direction of the aerodynamic pitching moment has no influence on the critical speed and the instability mode.
(3) The critical speed of the third failure mode is related only to the aerodynamic coefficient and is independent of the control gain parameters.

The three critical speeds proposed herein have important guiding significance for designing aerodynamic profiles and control schemes for new high-speed maglev trains. At present, reducing aerodynamic drag is the main objective in optimizing aerodynamic profile of maglev train. However, the aerodynamic profile optimized for aerodynamic drag may not be optimal for stability. Therefore, it is necessary to pay attention to this point that the large aerodynamic lift and pitching moment resulting from the aerodynamic profile with optimal drag may significantly reduce the critical speed of the train, thus reducing the motion stability of the train.

Acknowledgments

This project was supported by the National Key R&D Program of China (Grant 2016YFB1200602), the National Natural Science Foundation of China (Grants 51805522, 11672306 and 51490673), the Strategic Priority Research Program of the Chinese Academy of Sciences (Grant XDB22020100).

Appendix 1

m_c	the mass of the car body	39,000 m
I_c	the pitch inertia of the car body	175,450 kg•m^2
m_b	the mass of the maglev frame	8000 m
I_b	the pitch inertia of the maglev frame	6500 kg•m^2
k_s	the stiffness of a second suspension	2.05 × 10^{5}N/m
c_s	the damping of a second suspension	1.0 × 10^4 N•s/m
l_{cj}	the distance from the centre of the frame j to the centre of the car body	9.288 m (j = 1); 3.096 m (j = 2); −3.096 m (j = 3); −9.288 m (j = 4)
l_{bi}	the distance from the spring/damper i to the center of the maglev frame	1.548 m (i = 1); −1.548 m (i = 2)
l_{ek}	the distance from electromagnet k to the centre of the maglev frame	1.943 m (k = 1); 1.153 m (k = 2); −1.153 m (k = 3); −1.943 m (k = 4)
μ_0	the magnetic permeability of air	4π × 10^{-7} N/A^2
δ_0	the stable suspension clearance	0.01 m
N_m	the number of coil turns	290
R	the resistance coil turns	0.61Ω
A_m	the effective area of the electromagnet	0.311 m^2

Appendix 2

The other elements in the matrices **A, B**, and **K** that are not listed below are zero.

Matrix A $_{36\times36}$

A(1,2)=1;

$$A(2,1)=-8k_s/m_c,A(2,2)=-8c_s/m_c,A(2,3)=-\sum_{j=1}^{4}\sum_{i=1}^{2}[k_s(l_{cj}+l_{bi})]/m_c,$$

$$A(2,4)=-\sum_{j=1}^{4}\sum_{i=1}^{2}[c_s(l_{cj}+l_{bi})]/m_c,A(2,5)=2k_s/m_c,A(2,6)=2c_s/m_c,$$

$$A(2,7)=k_s(l_{b1}+l_{b2})/m_c,A(2,8)=c_s(l_{b1}+l_{b2})/m_c,A(2,9)=2k_s/m_c,A(2,10)=2c_s/m_c,$$

$$A(2,11)=k_s(l_{b1}+l_{b2})/m_c,A(2,12)=c_s(l_{b1}+l_{b2})/m_c,A(2,13)=2k_s/m_c,$$

$$A(2,14)=2c_s/m_c,A(2,15)=k_s(l_{b1}+l_{b2})/m_c,A(2,16)=c_s(l_{b1}+l_{b2})/m_c,$$

$$A(2,17)=2k_s/m_c,A(2,18)=2c_s/m_c,A(2,19)=k_s(l_{b1}+l_{b2})/m_c,$$

$$A(2,20)=c_s(l_{b1}+l_{b2})/m_c;$$

A(3,4)=1;

$$A(4,1)=-\sum_{j=1}^{4}\sum_{i=1}^{2}(l_{cj}+l_{bi})k_s/I_c,A(4,2)=-\sum_{j=1}^{4}\sum_{i=1}^{2}(l_{cj}+l_{bi})c_s/I_c,$$

$$A(4,3)=-\sum_{j=1}^{4}\sum_{i=1}^{2}(l_{cj}+l_{bi})^2k_s/I_c,A(4,4)=-\sum_{j=1}^{4}\sum_{i=1}^{2}(l_{cj}+l_{bi})^2c_s/I_c,$$

$$A(4,5)=\sum_{i=1}^{2}(l_{c1}+l_{bi})k_s/I_c,A(4,6)=\sum_{i=1}^{2}(l_{c1}+l_{bi})c_s/I_c,A(4,7)=\sum_{i=1}^{2}(l_{c1}+l_{bi})l_{bi}k_s/I_c,$$

$$A(4,8)=\sum_{i=1}^{2}(l_{c1}+l_{bi})l_{bi}c_s/I_c,A(4,9)=\sum_{i=1}^{2}(l_{c2}+l_{bi})k_s/I_c,A(4,10)=\sum_{i=1}^{2}(l_{c2}+l_{bi})c_s/I_c,$$

$$A\ (4,11)=\sum_{i=1}^{2}(l_{c2}+l_{bi})l_{bi}k_s/I_c,A(4,12)=\sum_{i=1}^{2}(l_{c2}+l_{bi})l_{bi}c_s/I_c,$$

$$A(4,13)=\sum_{i=1}^{2}(l_{c3}+l_{bi})k_s/I_c,A(4,14)=\sum_{i=1}^{2}(l_{c3}+l_{bi})c_s/I_c,$$

$$A(4,15)=\sum_{i=1}^{2}(l_{c3}+l_{bi})l_{bi}k_s/I_c,A(4,16)=\sum_{i=1}^{2}(l_{c3}+l_{bi})l_{bi}c_s/I_c,$$

$$A(4,17)=\sum_{i=1}^{2}(l_{c4}+l_{bi})k_s/I_c,A(4,18)=\sum_{i=1}^{2}(l_{c4}+l_{bi})c_s/I_c,$$

$$A(4,19)=\sum_{i=1}^{2}(l_{c4}+l_{bi})l_{bi}k_s/I_c,A(4,20)=\sum_{i=1}^{2}(l_{c4}+l_{bi})l_{bi}c_s/I_c;$$

A(5,6)=1;

$$A(6,1)=2k_s/m_b,A(6,2)=2c_s/m_b,A(6,3)=\sum_{i=1}^{2}k_s(l_{c1}+l_{bi})/m_b,$$

$$A(6,4)=\sum_{i=1}^{2}c_s(l_{c1}+l_{bi})/m_b,A(6,5)=[-2k_s-\sum_{k=1}^{4}(-k_{c,1k})]/m_b,$$

$$A(6,6)=-2c_s/m_b, A(6,7)=[-k_s(l_{b1}+l_{b2})-\sum_{k=1}^{4}(-k_{c,1k}l_{ek})]/m_b\ ,$$
$$A(6,8)=-c_s(l_{b1}+l_{b2})/m_b\ , A(6,21)=-k_{i,11}/m_b, A(6,22)=-k_{i,12}/m_b,$$
$$A(6,23)=-k_{i,13}/m_b, A(6,24)=-k_{i,14}/m_b;$$
$$A(7,8)=1;$$
$$A(8,1)=(l_{b1}+l_{b2})k_s/I_b, A(8,2)=(l_{b1}+l_{b2})c_s/I_b, A(8,3)=\sum_{i=1}^{2}l_{bi}k_s(l_{c1}+l_{bi})/I_b,$$
$$A(8,4)=\sum_{i=1}^{2}l_{bi}c_s(l_{c1}+l_{bi})/I_b, A(8,5)=[-(l_{b1}+l_{b2})k_s-\sum_{k=1}^{4}(-l_{ek}k_{c,1k})]/I_b,$$
$$A(8,6)=-(l_{b1}+l_{b2})c_s/I_b, A(8,7)=[-(l_{b1}^{\ 2}+l_{b2}^{\ 2})k_s-\sum_{k=1}^{4}(-l_{ek}^{\ 2}k_{c,1k})]/I_b,$$
$$A(8,8)=-(l_{b1}^{\ 2}+l_{b2}^{\ 2})c_s/I_b, A(8,21)=-l_{e1}k_{i,11}/I_b, A(8,22)=-l_{e2}k_{i,12}/I_b,$$
$$A(8,23)=-l_{e3}k_{i,13}/I_b, A(8,24)=-l_{e4}k_{i,14}/I_b;$$
$$A(9,10)=1;$$
$$A(10,1)=2k_s/m_b, A(10,2)=2c_s/m_b, A(10,3)=\sum_{i=1}^{2}k_s(l_{c2}+l_{bi})/m_b,$$
$$A(10,4)=\sum_{i=1}^{2}c_s(l_{c2}+l_{bi})/m_b, A(10,9)=[-2k_s-\sum_{k=1}^{4}(-k_{c,2k})]/m_b,$$
$$A(10,10)=-2c_s/m_b, A(10,11)[-k_s(l_{b1}+l_{b2})-\sum_{k=1}^{4}(-k_{c,2k}l_{ek})]/m_b\ ,$$
$$A(10,12)=-c_s(l_{b1}+l_{b2})/m_b\ , A(10,25)=-k_{i,21}/m_b, A(10,26)=-k_{i,22}/m_b,$$
$$A(10,27)=-k_{i,23}/m_b, A(10,28)=-k_{i,24}/m_b;$$
$$A(11,12)=1;$$
$$A(12,1)=(l_{b1}+l_{b2})k_s/I_b, A(12,2)=(l_{b1}+l_{b2})c_s/I_b,$$
$$A(12,3)=\sum_{i=1}^{2}l_{bi}k_s(l_{c2}+l_{bi})/I_b, A(12,4)=\sum_{i=1}^{2}l_{bi}c_s(l_{c2}+l_{bi})/I_b,$$
$$A(12,9)=[-(l_{b1}+l_{b2})k_s-\sum_{k=1}^{4}(-l_{ek}k_{c,2k})]/I_b, A(12,10)=-(l_{b1}+l_{b2})c_s/I_b,$$
$$A(12,11)=[-(l_{b1}^{\ 2}+l_{b2}^{\ 2})k_s-\sum_{k=1}^{4}(-l_{ek}^{\ 2}k_{c,2k})]/I_b,$$
$$A(12,12)=-(l_{b1}^{\ 2}+l_{b2}^{\ 2})c_s/I_b, A(12,25)=-l_{e1}k_{i,21}/I_b, A(12,26)=-l_{e2}k_{i,22}/I_b,$$
$$A(12,27)=-l_{e3}k_{i,23}/I_b, A(12,28)=-l_{e4}k_{i,24}/I_b;$$
$$A(13,14)=1;$$
$$A(14,1)=2k_s/m_b, A(14,2)=2c_s/m_b, A(14,3)=\sum_{i=1}^{2}k_s(l_{c3}+l_{bi})/m_b,$$
$$A(14,4)=\sum_{i=1}^{2}c_s(l_{c3}+l_{bi})/m_b, A(14,13)=[-2k_s-\sum_{k=1}^{4}(-k_{c,3k})]/m_b,$$
$$A(14,14)=-2c_s/m_b, A(14,15)=[-k_s(l_{b1}+l_{b2})-\sum_{k=1}^{4}(-k_{c,3k}l_{ek})]/m_b\ ,$$
$$A(14,16)=-c_s(l_{b1}+l_{b2})/m_b\ , A(14,29)=-k_{i,31}/m_b, A(14,30)=-k_{i,32}/m_b,$$
$$A(14,31)=-k_{i,33}/m_b, A(14,32)=-k_{i,34}/m_b;$$
$$A(15,16)=1;$$
$$A(16,1)=(l_{b1}+l_{b2})k_s/I_b, A(16,2)=(l_{b1}+l_{b2})c_s/I_b,$$
$$A(16,3)=\sum_{i=1}^{2}l_{bi}k_s(l_{c3}+l_{bi})/I_b, A(16,4)=\sum_{i=1}^{2}l_{bi}c_s(l_{c3}+l_{bi})/I_b,$$
$$A(16,13)=[-(l_{b1}+l_{b2})k_s-\sum_{k=1}^{4}(-l_{ek}k_{c,3k})]/I_b, A(16,14)=-(l_{b1}+l_{b2})c_s/I_b,$$
$$A(16,15)=[-(l_{b1}^{\ 2}+l_{b2}^{\ 2})k_s-\sum_{k=1}^{4}(-l_{ek}^{\ 2}k_{c,3k})]/I_b,$$
$$A(16,16)=-(l_{b1}^{\ 2}+l_{b2}^{\ 2})c_s/I_b, A(16,29)=-l_{e1}k_{i,31}/I_b, A(16,30)=-l_{e2}k_{i,32}/I_b,$$
$$A(16,31)=-l_{e3}k_{i,33}/I_b, A(16,32)=-l_{e4}k_{i,34}/I_b;$$
$$A(17,18)=1;$$
$$A(18,1)=2k_s/m_b, A(18,2)=2c_s/m_b, A(18,3)=\sum_{i=1}^{2}k_s(l_{c4}+l_{bi})/m_b,$$
$$A(18,4)=\sum_{i=1}^{2}c_s(l_{c4}+l_{bi})/m_b, A(18,17)=[-2k_s-\sum_{k=1}^{4}(-k_{c,4k})]/m_b,$$

$A(18,18)=-2c_s/m_b$,$A(18,19)=[-k_s(l_{b1}+l_{b2})-\sum_{k=1}^{4}(-k_{c,4k}l_{ek})]/m_b$,
$A(18,20)=-c_s(l_{b1}+l_{b2})/m_b$,$A(18,33)=-k_{i,41}/m_b$,$A(18,34)=-k_{i,42}/m_b$,
$A(18,35)=-k_{i,43}/m_b$,$A(18,36)=-k_{i,44}/m_b$;
$A(19,20)=1$;
$A(20,1)=(l_{b1}+l_{b2})k_s/I_b$,$A(20,2)=(l_{b1}+l_{b2})c_s/I_b$,
$A(20,3)=\sum_{i=1}^{2}l_{bi}k_s(l_{c4}+l_{bi})/I_b$,$A(20,4)=\sum_{i=1}^{2}l_{bi}c_s(l_{c4}+l_{bi})/I_b$,
$A(20,17)=[-(l_{b1}+l_{b2})k_s-\sum_{k=1}^{4}(-l_{ek}k_{c,4k})]/I_b$,$A(16,18)=-(l_{b1}+l_{b2})c_s/I_b$,
$A(20,19)=[-(l_{b1}{}^2+l_{b2}{}^2)k_s-\sum_{k=1}^{4}(-l_{ek}{}^2k_{c,4k})]/I_b$,
$A(20,20)=-(l_{b1}{}^2+l_{b2}{}^2)c_s/I_b$,$A(20,33)=-l_{e1}k_{i,41}/I_b$,$A(20,34)=-l_{e2}k_{i,42}/I_b$,
$A(20,35)=-l_{e3}k_{i,43}/I_b$,$A(20,36)=-l_{e4}k_{i,44}/I_b$;
$A(21,6)=\frac{k_{i,11}}{L_{0,11}}$,$A(21,8)=\frac{k_{i,11}}{L_{0,11}}l_{e1}$,$A(21,21)=-\frac{R}{L_{0,11}}$;
$A(22,6)=\frac{k_{i,12}}{L_{0,12}}$,$A(22,8)=\frac{k_{i,12}}{L_{0,12}}l_{e2}$,$A(22,22)=-\frac{R}{L_{0,12}}$;
$A(23,6)=\frac{k_{i,13}}{L_{0,13}}$,$A(23,8)=\frac{k_{i,13}}{L_{0,13}}l_{e3}$,$A(23,23)=-\frac{R}{L_{0,13}}$;
$A(24,6)=\frac{k_{i,14}}{L_{0,14}}$,$A(24,8)=\frac{k_{i,14}}{L_{0,14}}l_{e4}$,$A(24,24)=-\frac{R}{L_{0,14}}$;
$A(25,10)=\frac{k_{i,21}}{L_{0,21}}$,$A(25,12)=\frac{k_{i,21}}{L_{0,21}}l_{e1}$,$A(25,25)=-\frac{R}{L_{0,21}}$;
$A(26,10)=\frac{k_{i,22}}{L_{0,22}}$,$A(26,12)=\frac{k_{i,22}}{L_{0,22}}l_{e2}$,$A(26,26)=-\frac{R}{L_{0,22}}$;
$A(27,10)=\frac{k_{i,23}}{L_{0,23}}$,$A(27,12)=\frac{k_{i,23}}{L_{0,23}}l_{e3}$,$A(27,27)=-\frac{R}{L_{0,23}}$;
$A(28,10)=\frac{k_{i,24}}{L_{0,24}}$,$A(28,12)=\frac{k_{i,24}}{L_{0,24}}l_{e4}$,$A(28,28)=-\frac{R}{L_{0,24}}$;
$A(29,14)=\frac{k_{i,31}}{L_{0,31}}$,$A(29,16)=\frac{k_{i,31}}{L_{0,31}}l_{e1}$,$A(29,29)=-\frac{R}{L_{0,31}}$;
$A(30,14)=\frac{k_{i,32}}{L_{0,32}}$,$A(30,16)=\frac{k_{i,32}}{L_{0,32}}l_{e2}$,$A(30,30)=-\frac{R}{L_{0,32}}$;
$A(31,14)=\frac{k_{i,33}}{L_{0,33}}$,$A(31,16)=\frac{k_{i,33}}{L_{0,33}}l_{e3}$,$A(31,31)=-\frac{R}{L_{0,33}}$;
$A(32,14)=\frac{k_{i,34}}{L_{0,34}}$,$A(32,16)=\frac{k_{i,34}}{L_{0,34}}l_{e4}$,$A(32,32)=-\frac{R}{L_{0,34}}$;
$A(33,18)=\frac{k_{i,41}}{L_{0,41}}$,$A(33,20)=\frac{k_{i,41}}{L_{0,41}}l_{e1}$,$A(33,33)=-\frac{R}{L_{0,41}}$;
$A(34,18)=\frac{k_{i,42}}{L_{0,42}}$,$A(34,20)=\frac{k_{i,42}}{L_{0,42}}l_{e2}$,$A(34,34)=-\frac{R}{L_{0,42}}$;
$A(35,18)=\frac{k_{i,43}}{L_{0,43}}$,$A(35,20)=\frac{k_{i,43}}{L_{0,43}}l_{e3}$,$A(35,35)=-\frac{R}{L_{0,43}}$;
$A(36,18)=\frac{k_{i,44}}{L_{0,44}}$,$A(36,20)=\frac{k_{i,44}}{L_{0,44}}l_{e4}$,$A(36,36)=-\frac{R}{L_{0,44}}$.

Matrix B $_{36\times36}$

$B(21,21)=\frac{1}{L_{0,11}}$,$B(22,22)=\frac{1}{L_{0,12}}$,$B(23,23)=\frac{1}{L_{0,13}}$,$B(24,24)=\frac{1}{L_{0,14}}$;
$B(25,25)=\frac{1}{L_{0,21}}$,$B(26,26)=\frac{1}{L_{0,22}}$,$B(27,27)=\frac{1}{L_{0,23}}$,$B(28,28)=\frac{1}{L_{0,24}}$;
$B(29,29)=\frac{1}{L_{0,31}}$,$B(30,30)=\frac{1}{L_{0,32}}$,$B(31,31)=\frac{1}{L_{0,33}}$,$B(32,32)=\frac{1}{L_{0,34}}$;
$B(33,33)=\frac{1}{L_{0,41}}$,$B(34,34)=\frac{1}{L_{0,42}}$,$B(35,35)=\frac{1}{L_{0,43}}$,$B(36,36)=\frac{1}{L_{0,44}}$.

Matrix K $_{36\times36}$

$K(21,5)=k_p$,$K(21,6)=k_d$,$K(21,7)=k_pl_{e1}$,$K(21,8)=k_dl_{e1}$;
$K(22,5)=k_p$,$K(22,6)=k_d$,$K(22,7)=k_pl_{e2}$,$K(22,8)=k_dl_{e2}$;
$K(23,5)=k_p$,$K(23,6)=k_d$,$K(23,7)=k_pl_{e3}$,$K(23,8)=k_dl_{e3}$;
$K(24,5)=k_p$,$K(24,6)=k_d$,$K(24,7)=k_pl_{e4}$,$K(24,8)=k_dl_{e4}$;
$K(25,9)=k_p$,$K(25,10)=k_d$,$K(25,11)=k_pl_{e1}$,$K(25,12)=k_dl_{e1}$;
$K(26,9)=k_p$,$K(26,10)=k_d$,$K(26,11)=k_pl_{e2}$,$K(26,12)=k_dl_{e2}$;
$K(27,9)=k_p$,$K(27,10)=k_d$,$K(27,11)=k_pl_{e3}$,$K(27,12)=k_dl_{e3}$;
$K(28,9)=k_p$,$K(28,10)=k_d$,$K(28,11)=k_pl_{e4}$,$K(28,12)=k_dl_{e4}$;
$K(29,13)=k_p$,$K(29,14)=k_d$,$K(29,15)=k_pl_{e1}$,$K(29,16)=k_dl_{e1}$;
$K(30,13)=k_p$,$K(30,14)=k_d$,$K(30,15)=k_pl_{e2}$,$K(30,16)=k_dl_{e2}$;
$K(31,13)=k_p$,$K(31,14)=k_d$,$K(31,15)=k_pl_{e3}$,$K(31,16)=k_dl_{e3}$;
$K(32,13)=k_p$,$K(32,14)=k_d$,$K(32,15)=k_pl_{e4}$,$K(32,16)=k_dl_{e4}$;
$K(33,17)=k_p$,$K(33,18)=k_d$,$K(33,19)=k_pl_{e1}$,$K(33,20)=k_dl_{e1}$;
$K(34,17)=k_p$,$K(34,18)=k_d$,$K(34,19)=k_pl_{e2}$,$K(34,20)=k_dl_{e2}$;

$K(35,17)=k_p, K(35,18)=k_d, K(35,19)=k_p l_{e3}, K(35,20)=k_d l_{e3}$;
$K(36,17)=k_p, K(36,18)=k_d, K(36,19)=k_p l_{e4}, K(36,20)=k_d l_{e4}$.

References

[1] H.W. Lee, K.C. Kim, J. Lee, Review of maglev train technologies, IEEE Trans. Magn. 42 (7) (2006) 1917–1925.
[2] D.F. Zhou, C.H. Hansen, J. Li, W.S. Chang, Review of coupled vibration problems in EMS maglev vehicles, Int. J. Acoust. Vib. 15 (1) (2010) 10–23.
[3] Z.G. Huang, Study on Aerodynamics of Super High Speed Maglev Train, Southwest Jiaotong University, 2018 (in Chinese).
[4] D.B. Ma, Study on Pressure Wave and Aerodynamic Characteristics of a Maglev Train Passing through the Tunnel at 600km/h, Lanzhou Jiaotong University, 2018 (in Chinese).
[5] Y.G. Mei, H.B. Zhao, D.W. Chen, et al., Numerical simulation of initial compression wave characteristics of 600km/h maglev train entering tunnel, J. Traffic Transp. Eng. 20 (01) (2020) 120–131 (in Chinese).
[6] D.G. Gao, F. Ni, G.B. Lin, et al., Aerodynamic Analysis of Pressure Wave of High-Speed Maglev Vehicle Crossing Modeling and Calculation, Energies 12 (2019) 3770.
[7] S. Huang, Z.W. Li, M.Z. Yang, Aerodynamics of high-speed maglev trains passing each other in open air, J. Wind Eng. Ind. Aerodyn. 188 (2019) 151–160.
[8] P. Zhou, T. Li, C.F. Zhao, et al., Numerical study on the flow field characteristics of the new high-speed maglev train in open air, J. Zhejiang Univ. ENCE A 21 (5) (2020) 366–381.
[9] S.D. Kwon, J.S. Lee, J.W. Moon, M.Y. Kim, Dynamic interaction analysis of urban transit maglev vehicle and guide-way suspension bridge subjected to gusty wind, Eng. Struct. 30 (12) (2008) 3445–3456.
[10] J.D. Yau, Aerodynamic vibrations of a maglev vehicle running on flexible guide ways under oncoming wind actions, J. Sound Vib. 329 (10) (2010) 1743–1759.
[11] J.J. Wu, X.H. Shi, Numerical analyses of dynamic stability of maglev vehicles in crosswind field, J. Lanzhou Univ. Nat. Sci. 45 (2) (2009) 96–102 (in Chinese).
[12] T.H. Liu, H.Q. Tian, Transverse vibration analysis of two maglev trains passing by in open air, J. Traffic Transp. Eng. 5 (1) (2005) 39–44 (in Chinese).
[13] H. Takizawa, The vehicle dynamics characteristics of a magnetic levitation train passing another train running in opposite direction, Foreign Rolling Stock 41 (1) (2004) 30–33 (in Chinese).
[14] S.S. Ding, S.B. Yao, D.W. Chen, Aerodynamic lift force of high-speed maglev train, J. Mech. Eng. 56 (8) (2020) 228–234.
[15] H. Wu, X.H. Zeng, Y. Yu, Motion stability of high-speed maglev systems in consideration of aerodynamic effect: a study of a single magnetic suspension system, Acta Mech. Sin. 33 (6) (2017) 1084–1094.
[16] C.F. Zhao, W.M. Zhai, Maglev vehicle guide-way vertical random response and ride quality, Veh. Syst. Dyn. 38 (3) (2002) 185–210.
[17] D.J. Min, J.S. Lee, M.Y. Kim, Dynamic interaction analysis of actively controlled maglev vehicles and guideway girders considering nonlinear electromagnetic forces, Coupled Syst. Mech. 1 (1) (2012) 39–57.
[18] Y.Q. Deng, Static Levitation Stability Researches and Simulation of Maglev, Southwest Jiaotong University, 2002.
[19] J. Shi, Q.C. Wei, Y. Zhao, Analysis of dynamic response of the high-speed EMS maglev vehicle guideway coupling system with random irregularity, Veh. Syst. Dyn. 45 (12) (2007) 1077–1095.